CRYSTAL GROWTH & DESIGN

Article

pubs.acs.org/crystal

Syntheses, Crystal Structures, and Properties of Four Metal−Organic Complexes Based on 1,4,5,6,7,7-Hexachlorobicyclo[2.2.1]hept-5-ene-2,3-dicarboxylic Acid

Jie Yang,[‡] Xiaobin Liu,[†] Xiaoqing Wang,[‡] Fangna Dai,[*,†] Yan Zhou,[†] Bin Dong,[†] Liangliang Zhang,[†] Yanru Liu,[†] and Daofeng Sun[*,†]

[†]State Key Laboratory of Heavy Oil Processing, College of Science, China University of Petroleum (East China), Qingdao, Shandong 266580, People's Republic of China

[‡]Key Laboratory of Colloid and Interface Chemistry, Ministry of Education, School of Chemistry and Chemical Engineering, Shandong University, Jinan, Shandong 250100, People's Republic of China

Supporting Information

ABSTRACT: Four metal−organic complexes $[Ni(HET)(phen)(H_2O)]\cdot(HET)\cdot H_2O$ (**1**), $[Cu(HET)(phen)(H_2O)]\cdot 1.5H_2O$ (**2**), $[Cu_2(HET)_2(bipy)_{1.5}(H_2O)]\cdot 15DMF\cdot 2H_2O$ (**3**), and $[Cd_2O(HET)_2(bipy)(H_2O)]\cdot 2H_2O\cdot EtOH$ (**4**) (HET = 1,4,5,6,7,7-hexachlorobicyclo[2.2.1]hept-5-ene-2,3-dicarboxylic acid, phen = 1,10-phenanthroline, bipy = 4,4′-bipyridine) have been synthesized via hydro- or solvothermal reactions. It was found that complexes **1** and **2** are two-dimensional (2D) structures built from discrete complexes via the typical intermolecular interactions, and there was a closed loop built from the lattice water and carboxylate groups in **1** through intramolecular hydrogen bonds. Complex **3** exhibits three-dimensional (3D) structure with 5-connected ***bnn*** hexagonal BN topology. Complex **4** features a non-interpenetrating ***sql*** 2D coordination network, which is further linked into a 3D structure by C−H···Cl weak interaction. The properties of magnetism, fluorescence, and electrochemistry have also been investigated in this paper.

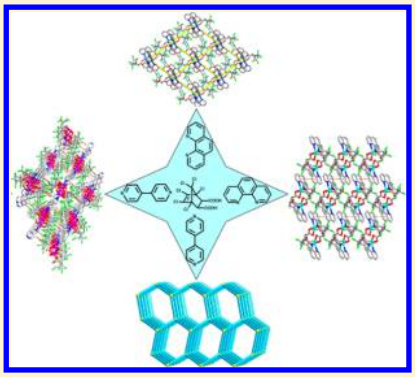

INTRODUCTION

In the past few years, the fascination of metal−organic complexes has attracted significant attention due to their potential applications in luminescence, magnetism, sensors, gas adsorption, conductivity, catalysis, and so on.[1−14] The self-assembly of metal−organic complexes may be influenced by many factors, such as central metal, organic ligand, temperature, pH, reaction time and solvent, etc.[15−19] Thus, the design and prediction of specific coordination structures are still a great scientific challenge.[20−24]

1,4,5,6,7,7-Hexachlorobicyclo[2.2.1]hept-5-ene-2,3-dicarboxylic acid (HET) (Scheme S1 in Supporting Information) functioning as the assembly ligand was chosen based on the following reasons: (a) the HET ligand could be assembled into chiral structures due to its chiral characteristic; (b) the two carboxylate groups in the HET ligand were linked by metal ions to generate high-dimensional or multinuclear complexes due to its diverse coordination modes; (c) six electrophilic chlorine atoms in the ligand act as hydrogen bond acceptors, which increase the possibilities of forming halogen and hydrogen bonds. And these bond interactions could play a key role in the self-assembly of metal−organic complexes.[25−27] Several organic coordination polymers such as $(C_{15}H_{12}Cl_6O_6)_x$, $(C_2H_4O)_n$-$(C_2H_4O)_nC_9H_4Cl_6O_4$, and $(C_{13}H_{10}Cl_6O_4)_n$ assembled with the HET ligand were reported.[28−30] However, a few studies on HET ligand coordinated with metal ions have been reported in recent years.[31,32] In particular, Berger's group studied HET coordinated with copper ion through the solvent extraction.[31] Recently, our group reported a new Cd-HET metal−organic complex via the solvothermal method.[32] However, most of the reported results focus on the structural and fluorescence properties. To further tap the properties of HET-based metal−organic complexes, we use the HET ligand in cooperation with with N-donor auxiliary ligands to assemble diverse metal ions in this paper. Hence, four new complexes based on HET were successfully synthesized through hydro- or solvothermal reactions. The structures were detected by single crystal X-ray crystallography, powder X-ray diffraction (PXRD), infrared (IR) spectroscopy, elemental analysis (EA), and thermogravimetric analysis (TGA). It was proposed that complexes **1** and **2** are built of discrete complexes, which were structured two-dimensional (2D) networks via C−H···O, C−H···Cl, and $\pi\cdots\pi$, C−H···Cl interactions, respectively. Complexes **3** and **4** are three-dimensional (3D) and 2D metal−organic complexes, respectively, and **4** was further linked into a 3D structure via C−H···Cl weak interaction. Furthermore, luminescent properties of complexes **1** and **4**, magnetic susceptibilities properties

Received: February 4, 2015
Revised: July 30, 2015
Published: August 6, 2015

DOI: 10.1021/acs.cgd.5b00164
Cryst. Growth Des. 2015, 15, 4198−4205

Table 1. Crystal Data for Complexes 1−4

complexes	1	2	3	4
formula	$C_{42}H_{26}Cl_{12}N_4O_{10}Ni$	$C_{21}H_{12}Cl_6N_2O_5Cu$	$C_{33}H_{18}Cl_{12}N_3O_9Cu_2$	$C_{30}H_{20}Cl_{12}N_2O_{11}Cd_2$
M_r	1230.78	648.57	1152.98	1234.68
crystal system	triclinic	triclinic	monoclinic	monoclinic
space group	$P\bar{1}$	$P\bar{1}$	$P2_1/c$	$P2_1/c$
a (Å)	12.1783(4)	8.492(8)	12.316(3)	13.7798(12)
b (Å)	12.6524(6)	12.824(12)	13.288(3)	12.6363(11)
c (Å)	16.6968(6)	13.253(13)	29.130(6)	25.0522(18)
α (deg)	95.897(3)	64.289(3)	90.00	90.00
β deg)	99.860(3)	72.003(16)	110.765(8)	114.451(4)
γ (deg)	104.902(4)	89.561(16)	90.00	90.00
Z	2	2	4	4
V (Å^3)	2420.2(17)	1223(2)	4457.8(17)	3971.0(6)
D_c (g cm^{-3})	1.689	1.761	1.718	2.065
μ (mm^{-1})	1.125	1.586	1.726	1.939
F (000)	1236.0	646.0	2284.0	2408.0
no. of unique reflns	17232	6240	21998	19468
no. of obsd reflns [$I > 2\sigma(I)$]	8625	4483	7856	7005
parameters	631	317	533	501
GOF	1.028	1.000	1.009	1.035
final R indices [$I > 2\sigma(I)$][a,b]	R_1 = 0.0584	R_1 = 0.0486	R_1 = 0.0588	R_1 = 0.0286
	wR_2 = 0.1498	wR_2 = 0.1136	wR_2 = 0.1450	wR_2 = 0.0725
R indices (all data)	R_1 = 0.0874	R_1 = 0.0789	R_1 = 0.0992	R_1 = 0.0347
	wR_2 = 0.1713	wR_2 = 0.1261	wR_2 = 0.1621	wR_2 = 0.0761
largest diff peak/hole/e Å^{-3}	0.41/−1.09	0.50/−0.45	1.31/−0.53	1.22/−1.00

[a] $R_1 = \Sigma||F_o| - |F_c||/\Sigma|F_o|$. [b] $wR_2 = [\Sigma w(F_o^2 - F_c^2)^2/\Sigma w(F_o^2)^2]^{0.5}$.

of the complexes **1**, **2**, and **3**, and basic electrochemical measurements of complexes **3** and **4** were also investigated.

EXPERIMENTAL SECTION

Materials and Methods. All chemical materials were obtained commercially and used without further purification. PXRD experiments were carried out with a Bruker AXS D8 Advance instrument. The IR spectra were obtained on a Nicolet 330 FTIR spectrometer in the range 4000−400 cm^{-1}. TGA were using a PerkinElmer TGA7 instrument. Photoluminescence spectra were recorded using an F-280 fluorescence spectrophotometer. EA (C, H, and N) was carried out on a PerkinElmer 240 elemental analyzer. The magnetic measurement was analyzed via the Squid-VSM Quantum Design. Electrochemical properties were measured on Gamry VFP 600 potentiostat.

Synthesis of [Ni(HET)(phen)(H_2O)]·(HET)·H_2O (1). $Ni(OAc)_2 \cdot 4H_2O$ (4.0 mg, 0.016 mmol), HET (2.0 mg, 0.005 mmol), and phen (1.0 mg, 0.006 mmol) in H_2O (1.0 mL) were sealed in a glass tube and heated to 90 °C for 48 h. Then the reaction system was cooled to room temperature slowly. Mauve virgulate crystals of **1** were obtained and dried in air at ambient temperature (yield: 50%, based on nickel). EA calcd (%) for **1**: $C_{42}H_{26}N_4O_{10}Cl_{12}Ni$: C, 40.99; H, 2.13; N, 4.55. Found: C, 40.62; H, 2.53; N, 4.88. IR data (KBr cm^{-1}): 3434 (w), 3062 (w), 2970 (w), 1731 (s), 1678 (m), 1606 (m), 1580 (s), 1518 (m), 1427 (s), 1197 (m), 1105 (w), 1065 (w), 883 (w), 841 (m), 727 (s), 659 (s), 620 (m).

Synthesis of [Cu(HET)(phen)(H_2O)]·1.5H_2O (2). $Cu(NO_3)_2 \cdot 3H_2O$ (4.0 mg, 0.017 mmol), HET (2.0 mg, 0.005 mmol), and phen (1.0 mg, 0.006 mmol) in EtOH-H_2O (1.0 mL, v/v = 2/1) were sealed in a glass tube and heated to 75 °C for 48 h. Then the reaction system was cooled to room temperature slowly. Blue virgulate crystals of **2** were obtained and dried in air at ambient temperature (yield: 40%, based on copper). EA calcd (%) for **2**: $C_{21}H_{15}O_{5.5}N_2Cl_6Cu$: C, 37.33; H, 2.24; N, 4.15. Found: C, 37.56; H, 1.99; N, 4.26. IR data (KBr cm^{-1}): 3429 (w), 3260 (w), 1629 (s), 1517 (w), 1400 (m), 1274 (w), 1174 (w), 1066 (w), 849 (m), 725 (m), 626 (m).

Synthesis of [Cu_2(HET)$_2$(4,4′-bipy)$_{1.5}$(H_2O)]·15DMF·2H_2O (3). $Cu(NO_3)_2 \cdot 3H_2O$ (4.0 mg, 0.017 mmol), HET (2.0 mg, 0.005 mmol), 4,4′-bpy (1.0 mg, 0.006 mmol) in DMF-EtOH-H_2O (1.0 mL, v/v/v = 1/1/1) were heated to 75 °C for 50 h in a sealed tube. The blue crystal plates formed on the wall of the glass tube were collected by filtration, washed with EtOH and dried in air (yield: 30%, based on copper). EA calcd (%) for **3**: $C_{78}H_{127}O_{26}N_{18}Cl_{12}Cu_2$: C, 40.99; H, 5.6; N, 12.03. Found: C, 41.23; H, 5.24; N, 12.15. IR spectrutrum (KBr, cm^{-1}): 3635 (w), 3270 (w), 1607 (s), 1542 (s), 1384 (s), 1260 (m), 1173 (w), 1067 (m), 893 (w), 841 (w), 818 (w), 664 (w), 632 (m).

Synthesis of [Cd_2O(HET)$_2$(4,4′-bipy)(H_2O)]·EtOH (4). $Cd(NO_3)_2 \cdot 4H_2O$ (4.0 mg, 0.013 mmol), HET (2.0 mg, 0.005 mmol), 4,4′-bpy (1.0 mg, 0.006 mmol) in EtOH-H_2O (1.0 mL, v/v = 2/1) were heated to 90 °C for 50 h in a sealed tube. The colorless block crystals were obtained and washed with EtOH (yield: 70%, based on cadmium). Elemental analysis calcd (%) for **4**: $C_{30}H_{20}O_{11}N_2Cl_{12}Cd_2$: C, 29.18; H, 1.63; N, 2.27. Found: C, 28.96; H, 1.32; N, 2.33. IR spectrutrum (KBr, cm^{-1}): 3566 (w), 3401 (w), 2971 (w), 2945 (w), 1747 (m), 1606 (s), 1392 (s), 1299 (w), 1204 (w), 1176 (m), 1066 (m), 895 (w), 846 (w), 821 (m), 663 (w), 629 (m), 478 (w).

Structural Crystallography. The structural data of **1**−**4** were collected on an Agilent SuperNova diffractometer with Cu−Kα radiation (λ = 1.54178 Å) and a Bruker SMART APEXII CCD Detector with graphite-monochromated Mo−Kα radiation source (λ = 0.71073 Å), respectively. Anisotropic parameters were performed in the refinement of all non-H atoms. Absorption corrections were applied with the program *SADABS*.[33] Structures were solved by direct method and refined by least-squares on F^2 using *SHELXTL*-97 routine.[34] Crystallographic data are presented in Table 1, and the selected bond lengths and bond angles are listed in Supporting Information, Table S1−S4. The topological analysis and some graphs were generated using the TOPOS program.[35] Crystallographic data have been deposited at the Cambridge Crystallographic Data Center, the numbers are 1063474, 1030264−1030266, respectively.

RESULTS AND DISCUSSION

Crystal Structure of Complex 1. The crystal data show that complex **1** is the triclinic system with $P\bar{1}$ space group. There are one Ni(II) ion, one coordinated HET ligand, two

DOI: 10.1021/acs.cgd.5b00164
Cryst. Growth Des. 2015, 15, 4198−4205

phen ligands, one coordinated water molecule, one lattice HET ligand, and one lattice water molecule in the asymmetric unit. As exhibited in Figure 1a, the Ni ion is located in an octahedron

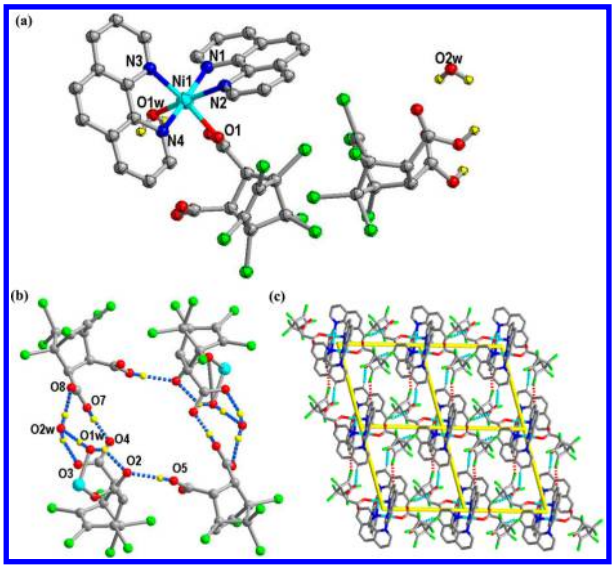

Figure 1. (a) Molecular structure of **1**. (b) The hydrogen bonds array in **1**. (c) The 2D structure formed by intermolecular C−H···O and C−H···Cl bond interactions.

configuration, which is coordinated by one O atom from HET ligand, four N atoms from two phen ancillary ligands and O1w from the water molecule. N1, N2, N4, and O1w are in the equatorial plane, and the vertical plane is bonded by O1 and N3. The average Ni−O bond distance is 2.083 Å, and Ni−N bond lengths range from 2.056 to 2.071 Å, which are consistent with the previous reports of nickel complexes.[36,37] Furthermore, lattice water molecule, coordinated water molecule, and two carboxylate groups from different ligands form a closed loop through hydrogen bonds, with H-bonds arrays of O8···O2w···O1w···O2···O5 and O8···O2w···O3, O4···O7. The O···O distances are fell in the range of 2.414−2.906 Å (Figure 1b). As depicted in Figure 1c, every adjacent structure unit is assembled into a 1D chain via two kinds of weak interactions, C−H···O (C24−H24···O4 = 3.154 Å) and C−H···Cl (C1−H1···Cl6 = 3.362 Å). Then, the 1D chains are further connected via C−H···O (C33−H33···O3 = 3.381 Å) weak interaction to generate a 2D structure. Two kinds of weak interactions are presented in this structure; the lengths conform to the values previously reported in the literature.[38]

Crystal Structure of Complex 2. Complex **2** crystallizes in triclinic space group $P\bar{1}$. The asymmetric unit contains one Cu(II) ion, one coordinated HET ligand, one auxiliary phen ligand, and one coordinated water molecule. As illustrated in Figure 2a, each Cu ion is coordinated by one chelating phen molecule, two oxygen atoms from HET ligand, and one coordination water molecule to form a slightly distorted square pyramidal geometry. The Cu−N1 bond distance is 2.244 Å in the axial positions, the bond distances range from 1.967 to 2.031 Å in the equatorial plane, and the bond angle range of vertex (N1) and four sides are 79.35−100.35°. In addition, a beautiful internal hydrogen bond exists in the Cu2 dimer (Cu···Cu distance is 5.071 Å); thereinto, the carboxylate oxygen from HET ligand and the H atom from the coordinated water molecule act as the receptor and donor, respectively. The H-

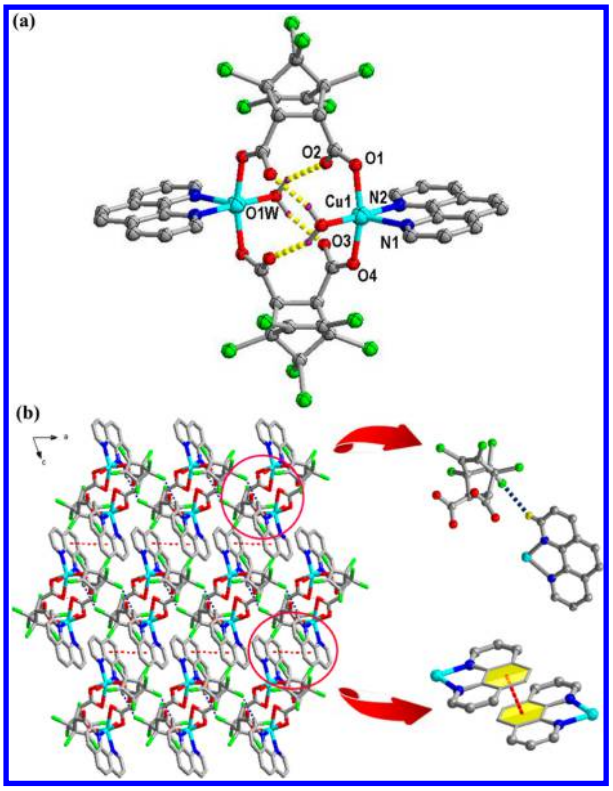

Figure 2. (a) The coordination environment of Cu(II) ion in **2**. (b) Ball and stick view of the 2D structure along the *b* axis formed by intermolecular interactions.

bonds array is O3···O1w···O2, and the O···O distances are 2.739 and 2.689 Å, respectively. Each adjacent structure unit generates a 1D chain through the $\pi\cdots\pi$ interaction; the distance of the approximate parallel planes from the stacks of two phen aromatic groups is about 3.846 Å. Then, every adjacent chain is interconnected into a 2D structure via C21−H21···Cl6 weak interaction (Figure 2b), and the H−Cl bond distance is 2.891 Å with the acceptable range of H−X bonds in previous reported complexes (2.569−2.944 Å).[39−41]

Crystal Structure of Complex 3. Complex **3** crystallizes in monoclinic space group $P2_1/n$. The asymmetric unit of **3** contains two independent Cu(II) ions, two HET ligands, one and a half 4,4′-bipy molecules, and one coordinated water molecule. Both Cu1 and Cu2 have the basal square-planar geometries. The Cu1 atom is bonded by two nitrogen atoms (N1 and N2) from two 4,4′-bipy molecules, and two oxygen atoms (O1 and O5) from two HET ligands with a N_2O_2 donor set. The Cu2 atom is connected by two O atoms (O3 and O8) from two different HET ligands, N3 atom from 4,4′-bipy molecule and O1w atom from coordinated water molecule with a NO_3 donor set (Figure 3a). During the reaction, both carboxylate groups of the ligand are deprotonated and adopt monodentate (η^1) modes. The average Cu−O and Cu−N distances are 1.957 and 2.007 Å, respectively. The Cu1···Cu2 distances are 6.392 and 6.125 Å, respectively, which are connected through the HET ligands, and 11.093 Å (connected by 4,4′-bipy). HET ligands bridged two central metal ions generate a 1D chain. Then the 1D chains are connected by 4,4′-bipy ligands to give rise to a 2D net (Figure 3b), which is further assembled into a 3D structure by the linkage of 4,4′-bipy ligands (Figure 3c). To be fully aware of the structure of complex **3**, we used the TOPOS software to execute topological

DOI: 10.1021/acs.cgd.5b00164
Cryst. Growth Des. 2015, 15, 4198−4205

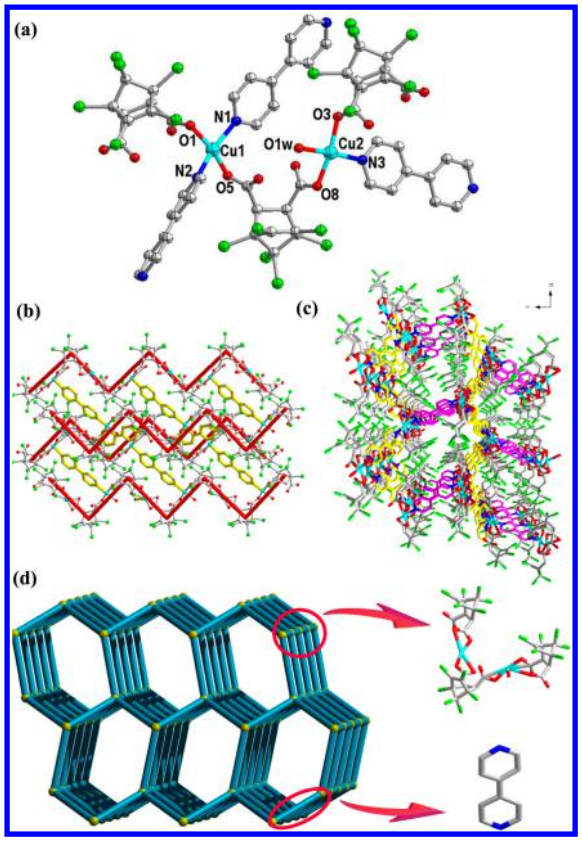

Figure 3. (a) and (b) The coordination environment of two Cu(II) ions and the 2D layer in **3** along the *a* axis. (c) and (d) The 3D structure and simplified 6-connected ***bnn*** topology of **3**.

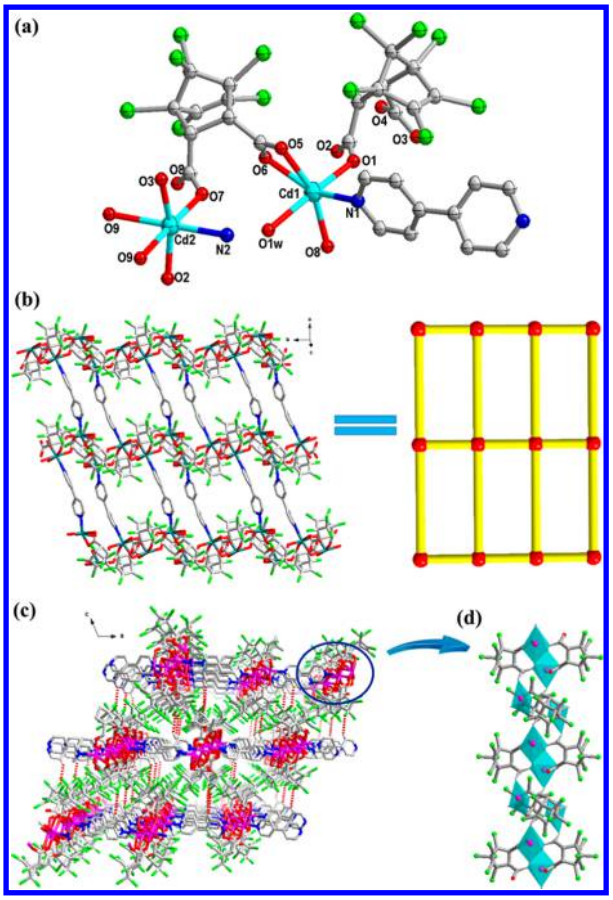

Figure 4. (a) The coordination environment of two Cd(II) ions in **4**. (b) Presentation of a 2D ***sql*** network. (c) The 3D structure formed by intermolecular C−H···Cl interaction (red dotted line). (d) The 1D chain in **4** formed by coordinated HET ligands and μ_2-bridge O atoms.

analysis of the complex.[42,43] As displayed in Figure 3d, the topological analysis reveals that the overall topology is a uninodal 5-connected 3D structure with $\{4^6.6^4\}$-***bnn*** hexagonal BN topology, upon defining Cu2 unit as a 5-connected node and the 4,4′-bipy ligand as linear linker.[44]

Crystal Structure of Complex 4. Complex **4** crystallizes in monoclinic space group $P2_1/c$; there are two Cd(II) ions, two HET ligands, one μ_2-O atom, one 4,4′-bipy molecule, and one coordinated water molecule in the asymmetric unit. As shown in Figure 4a, Cd1 is hexacoordinated in a distorted octahedral fashion, which is coordinated by four O atoms from three different HET ligands, O1w atom from water molecule (Cd−O = 2.272(4)−2.492(4) Å) with the coordination angles varying from 54.6(14)° to 164.14(17)°, and N1 atom from 4,4′-bipy molecule with Cd−N distance of 2.293 Å. The bond lengths around the Cd(II) ion are in good agreement with those typically observed.[45−47] Cd2 also adopt octahedral coordination environment, in which Cd2 is coordinated by three oxygen atoms from three different ligands, two μ_2-O atoms and an N2 atom from 4,4′-bipy molecule. The ligand possesses two types of coordination modes: μ^3-η^1:η^1:η^1:η^1 and μ^3-η^1:η^1:η^1:η^0. Two Cd^{II} ions are linked through carboxylate group from HET ligands and two μ_2-bridge O atoms to generate a 1D chain (Figure 4d), and then the chains are assembled into a 2D layer structure via the connection of 4,4′-bipy molecule (Figure 4b). As displayed in Figure 4c, there is a C−H···Cl weak interaction between two layers, which results in the formation of a 3D structure. The C−H···Cl bond distance is 2.935 Å within the commonly reported values (2.569−2.944 Å).[39−41] The whole 2D sheet can be seen as a 4-connected ***sql*** network with the Schäfli notation $\{4^4.6^2\}$.

X-ray Powder Diffraction Analyses, IR Spectra, Thermal Analyses, and Luminescent Properties. Complexes **1**−**4** were synthesized under different conditions in a seal glass tube by the solvothermal method, which has been demonstrated to be powerful in the assembly of metal−organic complexes.[48,49] All complexes are stable in the solid state upon exposure to air and have poor solubility in common organic solvents. PXRD was used to check the purity of the samples in the solid state. The measured PXRD patterns of four complexes closely match the simulated patterns generated from the results of single-crystal diffraction data by the mercury program, which indicated the four complexes were pure products (Figure S1). The IR spectra of HET ligand and four complexes are shown in Figure S2 (Supporting Information).

TGA experiments were performed in a N_2 atmosphere with a heating rate of 10 °C min^{-1} on polycrystalline samples of four complexes. The TGA curves are exhibited in Figure S3. The TGA curve of complex **1** shows a weight loss of 3.01% (calculated 2.92%) in the 29−192 °C range, which is attributed to the loss of one lattice water molecule and one coordinated water molecule. Further weight loss corresponding to uncoordinated HET ligand (observed 30.9%, calculated 31.6%) is observed between 192 and 360 °C. For complex **2**, from 32 to 172 °C, the weight loss of 4.02% is equivalent of losing one and a half water molecules (calculated 4.0%). The

DOI: 10.1021/acs.cgd.5b00164
Cryst. Growth Des. 2015, 15, 4198−4205

stability of the skeleton is observed for **3** in the temperature range of 32−172 °C, and the rather quick decomposition of **3** occurs with the temperature increasing. Complex **4** loses one ethanol molecule (observed 3.16%, calculated 3.89%) from 32 to 165 °C.

Generally, the coordination complexes of d^{10} transition metal centers have been exhibited photoluminescence applications in luminescent materials, chemical sensors, electroluminescent display, etc.[50−52] Meanwhile, the coordination modes of organic ligands and different metal ions also affect the emission wavelength and luminescent properties.[53] The fluorescence properties of complexes **1**, **4**, and free HET ligand have been measured in the solid state at room temperature, as depicted in Figure 5. And the photoluminescences of free phen and 4,4′-bipy have been displayed in Figure S4 upon the same excitation. The free HET ligand shows an intense emission band at 432 nm upon excitation at 330 nm, which may be attributed to $\pi^* \rightarrow$ n or $\pi^* \rightarrow \pi$ transition.[54,55] Under similar excitation condition, complexes **1** and **4** exhibit broad emission with maxima peaks at 463 and 440 nm, which are red-shifted by 31 nm, 8 nm in comparison to the free HET ligand, respectively. In addition, it is worth noting the change of luminescence for the complexes **1** and **4** compared with free ligand under the same conditions, which probably can be regarded as arising from the strong coordination interactions between the ligand and metal. Also, the results are rather of character typically observed for pair of ligand−ligand complexes.[56−58]

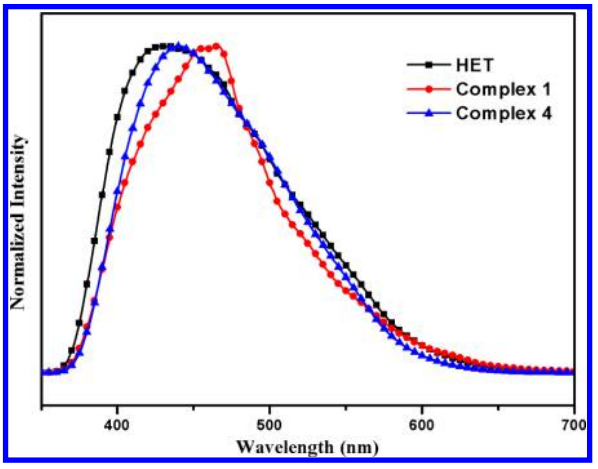

Figure 5. Photoluminescences of HET ligand, **1** and **4**.

Magnetic Property. The magnetic measurements of complexes **1**, **2**, and **3** were conducted at an applied magnetic field of 1000 Oe and in the temperature range of 1.8−300 K. The plot of $\chi_M T$ versus T of **1** is shown in Figure 6a; χ_M is the molar magnetic susceptibility per Ni^{II} unit. Complex **1** exhibits a dominant antiferromagnetic, and the values of $\chi_M T$ continually decrease as the temperature decreases and descends sharply after 16 K. The maximum $\chi_M T$ value is 0.94 $cm^3\ mol^{-1}$ K at 300 K, which is lower than the expected value (1 $cm^3\ mol^{-1}$ K, assuming g = 2.0).[59,60] The feature is antiferromagnetical behavior with weak antiferromagnetic interaction or zero-field-splitting (zfs). At high temperatures, the magnetic susceptibility follows the Curie−Weiss law ($\chi = C/(T - \theta)$), and the Curie−Weiss temperature estimated from the $\chi(T)$ dependence in the range 100−300 K, which is further supported by well-fitted χ_M^{-1} versus T plot that gives a Curie constant C = 0.96 $cm^3\ mol^{-1}$ K and Weiss constant θ = −9.08 K. The negative θ value for **1** also suggests an antiferromagnetic property. The effective magnetic moment μ_{eff} can be

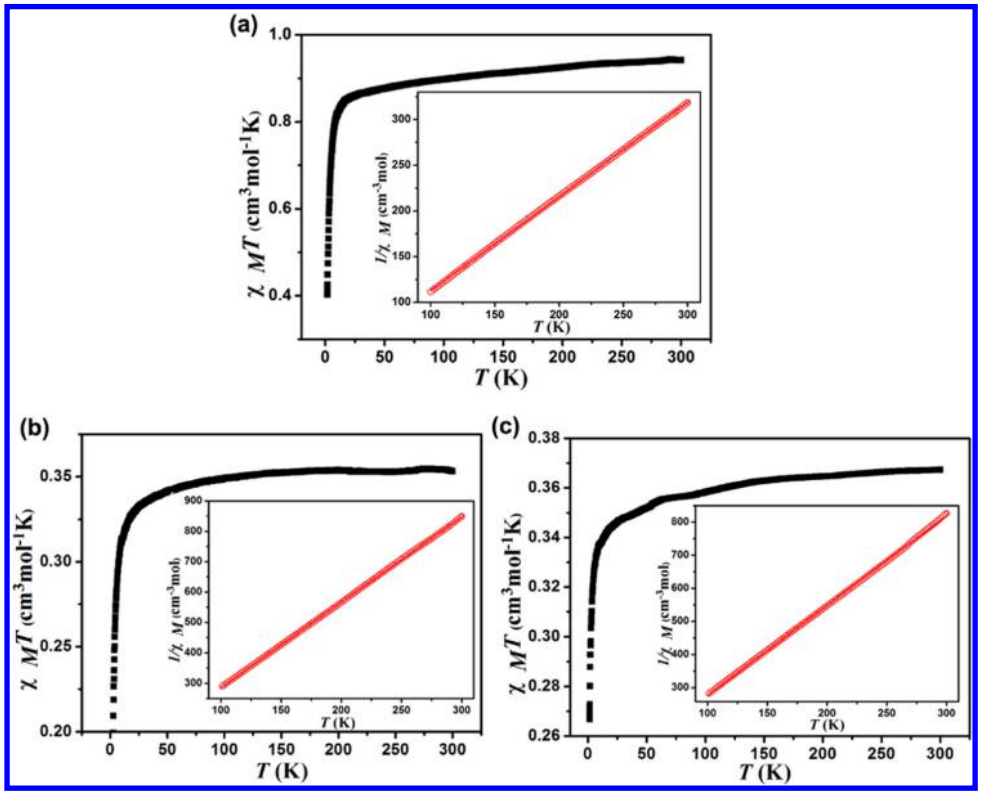

Figure 6. (a−c) Variable temperature susceptibility curve for complexes **1**, **2**, and **3**, respectively. The inset displaying $1/\chi_M$ versus T is the Curie−Weiss fitting, respectively.

DOI: 10.1021/acs.cgd.5b00164
Cryst. Growth Des. 2015, 15, 4198−4205

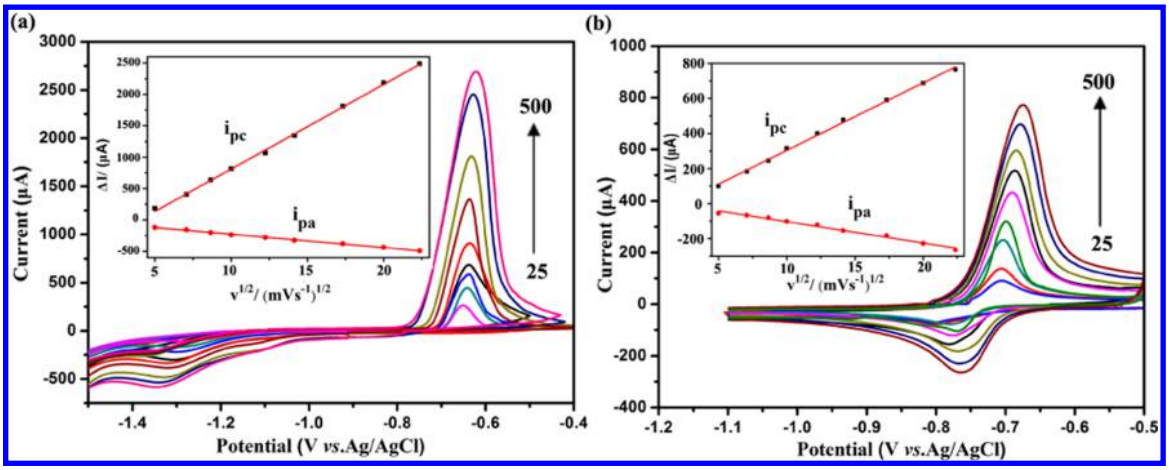

Figure 7. Cyclic voltammograms of **3** (a) and **4** (b) at variable of scan rates: 25, 50, 75, 100, 150, 200, 300, 400, 500 mV s^{-1}. Inset: the relationship of redox peak current and square root of scan rate.

approximated from the Curie constant with $\mu_{eff}^2 = 3k_BC/\mu_B^2N_A$, where k_B is the Boltzmann constant, μ_B is the Bohr magneton, and N_A is the Avogadro number. The value of μ_{eff} is 2.74 μ_B at 300 K, which is in agreement with theoretical estimations. We supposed the magnetic behavior in **1** is only associated with Ni^{2+} ($S = 1$) ion, $\mu_{theor}^2 = g^2\mu_B^2nS(S + 1)$, and we determined the g (lande factor) is 1.94.

In complex **2**, the Cu···Cu distance is 5.071 Å, which is connected by the organic ligand. For **2**, the χ_MT value is 0.35 cm^3 K mol^{-1} at 300 K, which corresponds to the single spin-state Cu^{II} ion. The room temperature magnetic moment is lower than the theoretical one (0.375 cm^3 mol^{-1} K, assuming g = 2.0). The χ_MT value decreases slightly in the 300−20 K range. Below 20 K, the χ_MT value descends rapidly, reaching a value of 0.21 cm^3 K mol^{-1} at 1.8 K, and it explains a very weak antiferromagnetic behavior exists in the complex (Figure 6b). The datum shows a linear behavior in 100−300 K range and obeys the Curie−Weiss law, $\chi = C/(T - \theta)$, with C = 0.36 cm^3 mol^{-1} K and θ = −1.67 K. The negative θ value for **2** also suggests an antiferromagnetic property. The value of the effective magnetic moment μ_{eff} is 1.67 μ_B at 300 K, and through the calculation of formula the value of Lande factor is 1.93 (Cu^{2+}, $S = 1/2$).

There are three kinds of Cu···Cu distances in complex **3**, two types connected by two different organic ligands (6.392 and 6.125 Å), respectively, and another connected by 4,4′-bipy (11.093 Å). For **3**, the χ_MT value is 0.36 cm^3 K mol^{-1} at 300 K, which is lower than the value expected for single high-spin Cu^{II} ion (0.375 cm^3 mol^{-1} K, assuming g = 2.0).[61,62] The χ_MT value slowly decreases to 0.34 cm^3 K mol^{-1} at 15 K and then descends more sharply, reaching a value of 0.27 cm^3 K mol^{-1} at 1.8 K. It indicates a very weak antiferromagnetic behavior presented in the complex. The inverse magnetic susceptibility curve shows a linear behavior in 100−300 K range and can be fitted to the Curie−Weiss law, $\chi = C/(T - \theta)$, yielding C = 0.37 cm^3 mol^{-1} K and θ = −2.24 K. The negative θ value for **3** also suggests an antiferromagnetic property, the same as **1** and **2**. As shown in Figure 6c, the value of the effective magnetic moment μ_{eff} is 1.70 μ_B at 300 K, and through the calculation of formula the value of Lande factor is 1.98.

The M−H magnetization data for three complexes were measured at 1.8 K, and an applied field ranged from −7 to 7 T. The data are shown in Figure S5, The magnetization values of three complexes are 1.9 μ_B, 0.79 μ_B, and 0.83 μ_B at 7 T, respectively. The magnetization values increased as the change of applied field. These results indicate a rather weak exchange between the metal centers in complexes **2** and **3**.[63−65]

Solid State Electrochemical Property. In order to examine the redox process of the metal ions in the complexes, the cyclic voltammetry experiments of the four complexes were performed, but only complexes **3** and **4** have redox peaks under aqueous potential window. The detailed preparation procedures are depicted in the Supporting Information. As illustrated in Figure 7, the cyclic voltammograms display that **3** and **4** donate reversible redox processes in the voltage scan ranging from −0.4 V to −1.6 V and −1.1 V to −0.5 V vs Ag/AgCl, respectively. The anodic peak potential for **3** appears at −0.62 V vs Ag/AgCl, and the corresponding cathodic peak potential was found to be −1.35 V vs Ag/AgCl, and $E_{1/2}$ = −0.67 and −1.17 V values for the framework are observed at 100 mV s^{-1} scan rate. The anodic peak potential for complex **4** is shown at −0.67 V vs Ag/AgCl, and the cathodic peak potential is shown at −0.76 V vs Ag/AgCl, and $E_{1/2}$ = −0.73 and −0.87 V values for the framework are observed at 100 mV s^{-1} scan rate. Moreover, the tests for cyclic voltammetry of **3** and **4** are performed at various scan rates ranging from 25 to 500 mV s^{-1} as shown in the inset of Figure 7, panels a and b, respectively. The peak current for both oxidation and reduction processes showing a linear relationship with square root of scan rate indicates that the redox process of complexes **3** and **4** are governed by diffusion.[66] According to studies by Trnková's group[67] and Llabrés-i-Xamena's group,[68] we found that the curves of the literature studies were similar to the curves of complexes **3** and **4**, and these phenomena could be attributed to the metal-centered redox process.

■ CONCLUSIONS

In summary, four complexes have been obtained through the solvothermal reactions of HET ligand and different N-donor auxiliary ligands coordinated with Ni(II), Cu(II), and Cd(II) salts. The results of these complexes are outlined as follows: (1) The discrete complexes are built in the synthetic process because the phen ligand adopts the chelating mode. Complexes **1** and **2** are discrete complexes, which are 2D structures built via the typical intermolecular interactions. (2) Because of the formation of complexes involves a pillar insertion strategy (4,4′-bipyridine), the 2D or 3D framework would be easily generated. Complex **3** exhibits a 3D open framework with a

DOI: 10.1021/acs.cgd.5b00164
Cryst. Growth Des. 2015, 15, 4198−4205

reported uninodal 5-connected ***bnn*** hexagonal BN topology. Complex **4** features a normal mode of uninodal 4-connected ***sql*** framework, which is further linked into a 3D structure via C−H···Cl weak interaction. (3) Using nickel and copper ions to assemble with organic ligand is advantageous for the formation of magnetic materials because both nickel and copper ions have the single ion (Ni, $S = 1$ spin state and Cu, $S = 1/2$ spin state). The magnetic results reveal that the magnetic behaviors of **1**, **2**, and **3** are antiferromagnetic, and thereinto, a rather weak exchange between the metal centers exists in complex **3**. (4) Because the ligand has six electrophilic chlorine atoms, the complexes based on the HET ligand may be of the mechanism of charge transport. The electrochemical experimental results show that complexes **3** and **4** possess the signals of a reversible redox process. Further study will focus on the synthesis of lanthanide metal−organic complexes based on the HET ligand and research on their luminescence and solid-state electrochemical properties.

■ ASSOCIATED CONTENT

Supporting Information

The Supporting Information is available free of charge on the ACS Publications website at DOI: 10.1021/acs.cgd.5b00164.

X-ray crystallographic data in CIF format, tables of bond distances and angles, PXRD patterns, FT-IR spectra, TG−DSC curves, M−H curves, and solid state electrochemistry (PDF)

X-ray crystallographic data (CIF)

■ AUTHOR INFORMATION

Corresponding Authors

*(D.S.) E-mail: dfsun@upc.edu.cn.

*(F.D.) E-mail: fndai@upc.edu.cn.

Funding

This work was supported by the National Natural Science Foundation of China (Grant Nos. 21271117, 21201179), China Postdoctoral Science Foundation (2014T70665), and the Fundamental Research Funds for the Central Universities (13CX05015A, 13CX05010A, 14CX02213A, 14CX02154A).

Notes

The authors declare no competing financial interest.

■ REFERENCES

(1) Sangeetha, N. M.; Maitra, U. *Chem. Soc. Rev.* **2005**, *34*, 821−836.

(2) Li, C. P.; Du, M. *Chem. Commun.* **2011**, *47*, 5958−5972.

(3) Moulton, B.; Zaworotko, M. J. *Chem. Rev.* **2001**, *101*, 1629−1658.

(4) Yin, Z.; Wang, Q. X.; Zeng, M. H. *J. Am. Chem. Soc.* **2012**, *134*, 4857−4863.

(5) Rusanov, E. B.; Ponomarova, V. V.; Komarchuk, V. V.; Stoeckli-Evans, H.; Fernandez-Ibanez, E.; Stoeckli, F.; Sieler, J.; Domasevitch, K. V. *Angew. Chem., Int. Ed.* **2003**, *42*, 2499−2501.

(6) Chen, B.; Xiang, S.; Qian, G. *Acc. Chem. Res.* **2010**, *43*, 1115−1124.

(7) Zeng, M. H.; Yao, M. X.; Liang, H.; Zhang, W. X.; Chen, X. M. *Angew. Chem., Int. Ed.* **2007**, *46*, 1832−1835.

(8) Daniel, M.; Astruc, D. *Chem. Rev.* **2004**, *104*, 293−346.

(9) O'Keeffe, M.; Yaghi, O. M. *Chem. Rev.* **2012**, *112*, 675−702.

(10) Talin, A. A.; Centrone, A.; Ford, A. C.; Foster, M. E.; Stavila, V.; Haney, P.; Kinney, R. A.; Szalai, V.; El Gabaly, F.; Yoon, H. P.; Leonard, F.; Allendorf, M. D. *Science* **2014**, *343*, 66−69.

(11) Zhou, X. P.; Liu, J.; Zhan, S. Z.; Yang, J. R.; Li, D.; Ng, K. M.; Sun, R. W. Y.; Che, C. M. *J. Am. Chem. Soc.* **2012**, *134*, 8042−8045.

(12) Chen, L.; Jiang, F.; Lin, Z.; Zhou, Y.; Yue, C.; Hong, M. *J. Am. Chem. Soc.* **2005**, *127*, 8588−8589.

(13) Zhao, X. L.; Liu, F. L.; Zhang, L. L.; Sun, D.; Wang, R. M.; Ju, Z. F.; Yuan, D. Q.; Sun, D. F. *Chem. - Eur. J.* **2014**, *20*, 649−652.

(14) Peng, P.; Li, F. F.; Neti, V.; Metta-Magana, A. J.; Echegoyen, L. *Angew. Chem., Int. Ed.* **2014**, *53*, 160−163.

(15) Xuan, W. M.; Zhang, M. N.; Liu, Y.; Chen, Z. J.; Cui, Y. *J. Am. Chem. Soc.* **2012**, *134*, 6904−6907.

(16) Farha, O. K.; Yazaydin, A. O.; Eryazici, I.; Malliakas, C.; Hauser, B.; Kanatzidis, M. G.; Nguyen, S. T.; Snurr, R. Q.; Hupp, J. T. *Nat. Chem.* **2010**, *2*, 944−948.

(17) Qiu, W.; Perman, J. A.; Wojtas, L.; Eddaoudi, M.; Zaworotko, M. J. *Chem. Commun.* **2010**, *46*, 8734−8736.

(18) Eliseeva, S. V.; Buenzli, J.-C. G. *Chem. Soc. Rev.* **2010**, *39*, 189−227.

(19) Sun, D.; Wei, Z. H.; Yang, C. F.; Wang, D. F.; Zhang, N.; Huang, R. B.; Zheng, L. S. *CrystEngComm* **2011**, *13*, 1591−1601.

(20) Bi, W. H.; Cao, R.; Sun, D. F.; Yuan, D. Q.; Li, X.; Wang, Y. Q.; Li, X. J.; Hong, M. C. *Chem. Commun.* **2004**, 2104−2105.

(21) Allendorf, M. D.; Bauer, C. A.; Bhakta, R. K.; Houk, R. J. T. *Chem. Soc. Rev.* **2009**, *38*, 1330−1352.

(22) Bergmann, O.; Bhardwaj, R. D.; Bernard, S.; Zdunek, S.; Barnabé-Heider, F.; Walsh, S.; Zupicich, J.; Alkass, K.; Buchholz, B. A.; Druid, H.; Jovinge, S.; Frisén, J. *Science* **2009**, *324*, 98−102.

(23) Zhang, J. P.; Huang, X. C.; Chen, X. M. *Chem. Soc. Rev.* **2009**, *38*, 2385−2396.

(24) Metrangolo, P.; Meyer, F.; Pilati, T.; Resnati, G.; Terraneo, G. *Angew. Chem., Int. Ed.* **2008**, *47*, 6114−6127.

(25) Berl, V.; Schmutz, M.; Krische, M. J.; Khoury, R. G.; Lehn, J. M. *Chem. - Eur. J.* **2002**, *8*, 1227−1244.

(26) Metrangolo, P.; Meyer, F.; Pilati, T.; Resnati, G.; Terraneo, G. *Angew. Chem., Int. Ed.* **2008**, *47*, 6114−6127.

(27) Dai, F. N.; He, H. Y.; Zhao, X. L.; Ke, Y. X.; Zhang, G. Q.; Sun, D. F. *CrystEngComm* **2010**, *12*, 337−340.

(28) Herr, D. E.; Kong, S. Q.; Gillissen, S. U.S. Patent Appl. Publ. 2007, U.S. 20070117917 A1 20070524.

(29) Takei, M.; Asao, Y.; Ito, O.; Tamura, M. Jpn. Kokai Tokkyo Koho 1999, JP 11228803 A 19990824.

(30) Vijayakumar, C. T.; Lederer, K. *Thermochim. Acta* **1990**, *173*, 129−135.

(31) Berger, S. A. *Talanta* **1976**, *23*, 475−477.

(32) Cui, P. P.; Cui, L. F.; Zhang, L. L.; Sun, D. F. *Z. Anorg. Allg. Chem.* **2013**, *639*, 1269−1273.

(33) *SMART, Saint and SADABS*; Bruker AXS Inc.: Madison, Wisconsin, USA, 1998.

(34) Sheldrick, G. M. *SHELXS-97, Program for X-ray Crystal Structure Determination*; University of Gottingen: Germany, 1997.

(35) Blatov, V. A.; Shevchenko, A. P.; Serezhkin, V. N. *J. Appl. Crystallogr.* **2000**, *33*, 1193.

(36) Karra, J. R.; Huang, Y. G.; Walton, K. S. *Cryst. Growth Des.* **2013**, *13*, 1075−1081.

(37) Nagaraja, C. M.; Haldar, R.; Maji, T. K.; Rao, C. N. R. *Cryst. Growth Des.* **2012**, *12*, 975−981.

(38) Banerjee, R.; Mondal, R.; Howard, J. K.; Desiraju, G. R. *Cryst. Growth Des.* **2006**, *6*, 999−1009.

(39) Taylor, R.; Kennard, O. *J. Am. Chem. Soc.* **1982**, *104*, 5063−5070.

(40) Balamurugan, V.; Jacob, W.; Mukherjee, J.; Mukherjee, R. *CrystEngComm* **2004**, *6*, 396−400.

(41) Balamurugan, V.; Hundal, M. S.; Mukherjee, R. *Chem. - Eur. J.* **2004**, *10*, 1683−1690.

(42) Gong, Y.; Jiang, P. G.; Li, Q. F.; Lin, J. H.; Li, J. *Dalton Trans.* **2013**, *42*, 1603−1611.

(43) Blatov, V. A. *Struct. Chem.* **2012**, *23*, 955−963.

(44) Delgado Friedrichs, O.; O'Keeffe, M.; Yaghi, O. M. *Acta Crystallogr., Sect. A: Found. Crystallogr.* **2003**, *59*, 22−27.

(45) Li, B.; Peng, Y.; Li, B.; Zhang, Y. *Chem. Commun.* **2005**, 2333−2335.

DOI: 10.1021/acs.cgd.5b00164
Cryst. Growth Des. 2015, 15, 4198−4205

(46) Wang, R.; Han, L.; Jiang, F.; Zhou, Y.; Yuan, D.; Hong, M. *Cryst. Growth Des.* **2005**, *5*, 129−135.
(47) Cheng, J. Y.; Dong, Y. B.; Huang, R. Q.; Smith, M. D. *Inorg. Chim. Acta* **2005**, *358*, 891−902.
(48) Zhou, J. M.; Shi, W.; Xu, N.; Cheng, P. *Inorg. Chem.* **2013**, *52*, 8082−8090.
(49) Sun, D.; Xu, M. Z.; Liu, S. S.; Lu, H. F.; Feng, S. Y.; Sun, D. F.; Yuan, S. *Dalton Trans.* **2013**, *42*, 12324−12333.
(50) Cui, Y. J.; Yue, Y. F.; Qian, G. D.; Chen, B. L. *Chem. Rev.* **2012**, *112*, 1126−1162.
(51) Qiu, Y. C.; Li, Y. H.; Peng, G.; Cai, J. B.; Jin, L. M.; Ma, L.; Deng, H.; Zeller, M.; Batten, S. R. *Cryst. Growth Des.* **2010**, *10*, 1332−1340.
(52) Jiang, H. L.; Liu, B.; Xu, Q. *Cryst. Growth Des.* **2010**, *10*, 806−811.
(53) Colacio, E.; Kivekäs, R.; Lloret, F.; Sunberg, M.; Suarez-Varela, J.; Bardají, M.; Laguna, A. *Inorg. Chem.* **2002**, *41*, 5141−5149.
(54) Cui, P.; Chen, Z.; Gao, D. L.; Zhao, B.; Shi, W.; Cheng, P. *Cryst. Growth Des.* **2010**, *10*, 4370−4378.
(55) Shi, X.; Zhu, G. S.; Fang, Q. R.; Wu, G.; Tian, G.; Wang, R. W.; Zhang, D. L.; Xue, M.; Qiu, S. L. *Eur. J. Inorg. Chem.* **2004**, *2004*, 185−191.
(56) Cui, L.; Luan, X. J.; Zhang, C. P.; Kang, Y. F.; Zhang, W. T.; Wang, Y. Y.; Shi, Q. Z. *Dalton Trans* **2013**, *42*, 1637−1644.
(57) Fang, S. M.; Zhang, Q.; Hu, M.; Yang, X. G.; Zhou, L. M.; Du, M.; Liu, C. S. *Cryst. Growth Des.* **2010**, *10*, 4773−4785.
(58) Zhang, Y. N.; Liu, P.; Wang, Y. Y.; Wu, L. Y.; Pang, L. Y.; Shi, Q. Z. *Cryst. Growth Des.* **2011**, *11*, 1531−1541.
(59) Habib, H. A.; Sanchiz, J.; Janiak, C. *Dalton Trans.* **2008**, 1734−1744.
(60) Zvereva, E. A.; Evstigneeva, M. A.; Nalbandyan, V. B.; Savelieva, O. A.; Ibragimov, S. A.; Volkova, O. S.; Medvedeva, L. I.; Vasiliev, A. N.; Klingeler, R.; Buechner, B. *Dalton Trans.* **2012**, *41*, 572−580.
(61) Vasylevs'kyy, S. I.; Senchyk, G. A.; Lysenko, A. B.; Rusanov, E. B.; Chernega, A. N.; Jezierska, J.; Krautscheid, H.; Domasevitch, K. V.; Ozarowski, A. *Inorg. Chem.* **2014**, *53*, 3642−3654.
(62) Escobar, L. B. L.; Guedes, G. P.; Soriano, S.; Speziali, N. L.; Jordao, A. K.; Cunha, A. C.; Ferreira, V. F.; Maxim, C.; Novak, M. A.; Andruh, M.; Vaz, M. G. F. *Inorg. Chem.* **2014**, *53*, 7508−7517.
(63) Colacio, E.; Ghazi, M.; Kivekäs, R.; Moreno, J. M. *Inorg. Chem.* **2000**, *39*, 2882−2890.
(64) Ikeue, T.; Sawada, N.; Matsumoto, N.; Miyazaki, A.; Sugimori, T.; Koikawa, M.; Hiromitsu, I.; Yoshino, K.; Mikuriya, M.; Kataoka, Y.; Handa, M. *J. Porphyrins Phthalocyanines* **2014**, *18*, 708−714.
(65) Khullar, S.; Mandal, S. K. *Cryst. Growth Des.* **2014**, *14*, 6433−6444.
(66) Mao, J. J.; Yang, L. F.; Yu, P.; Wei, X.; Mao, L. *Electrochem. Commun.* **2012**, *19*, 29−31.
(67) Rozik, R.; Trnková, L. *J. Electroanal. Chem.* **2006**, *593*, 247−257.
(68) Doménech, A.; García, H.; Doménech-Carbó, M. T.; Llabrés-i-Xamena, F. *Electrochem. Commun.* **2006**, *8*, 1830−1834.

DOI: 10.1021/acs.cgd.5b00164
Cryst. Growth Des. 2015, 15, 4198−4205